# Supporting Information

# Energy yield modelling of perovskite/silicon two-terminal tandem PV modules with flat and textured interfaces

*Jonathan Lehr*[†,a,]*, *Malte Langenhorst*[†, b], *Raphael Schmager*[b], *Simon Kirner*[c], *Uli Lemmer*[a,b], *Bryce S. Richards*[a,b], *Chris Case*[c], *Ulrich W. Paetzold*[a,b,]*

[a] *Light Technology Institute, Karlsruhe Institute of Technology, Engesserstrasse 13, 76131 Karlsruhe, Germany*
[b] *Institute of Microstructure Technology, Karlsruhe Institute of Technology, Hermann-von-Helmholtz-Platz 1, 76344 Eggenstein-Leopoldshafen, Germany*
[c] *Oxford Photovoltaics, Unit 7-8 Oxford Industrial Park, Mead Road, Oxford, OX5 1QU, United Kingdom*

## Methods

The energy yield (EY) modelling is based on an in-house developed code, that combines: i) an optics software module for the rigorous optical simulation of the current generation in the solar cell; ii) an irradiance software module that generates angular and wavelength-resolved irradiance data for various locations in the USA; iii) an electrical software module that determines the current-density versus voltage (*J-V*) characteristics of the solar cell; and, finally, iv) the EY software module itself. A schematic of the software modules is provided in Figure S1. It should be noted, that in this contribution the optical aspects are in the focus and other effects such as the temperature of the perovskite/Si two-terminal (2T) tandem photovoltaics (PV) are disregarded.

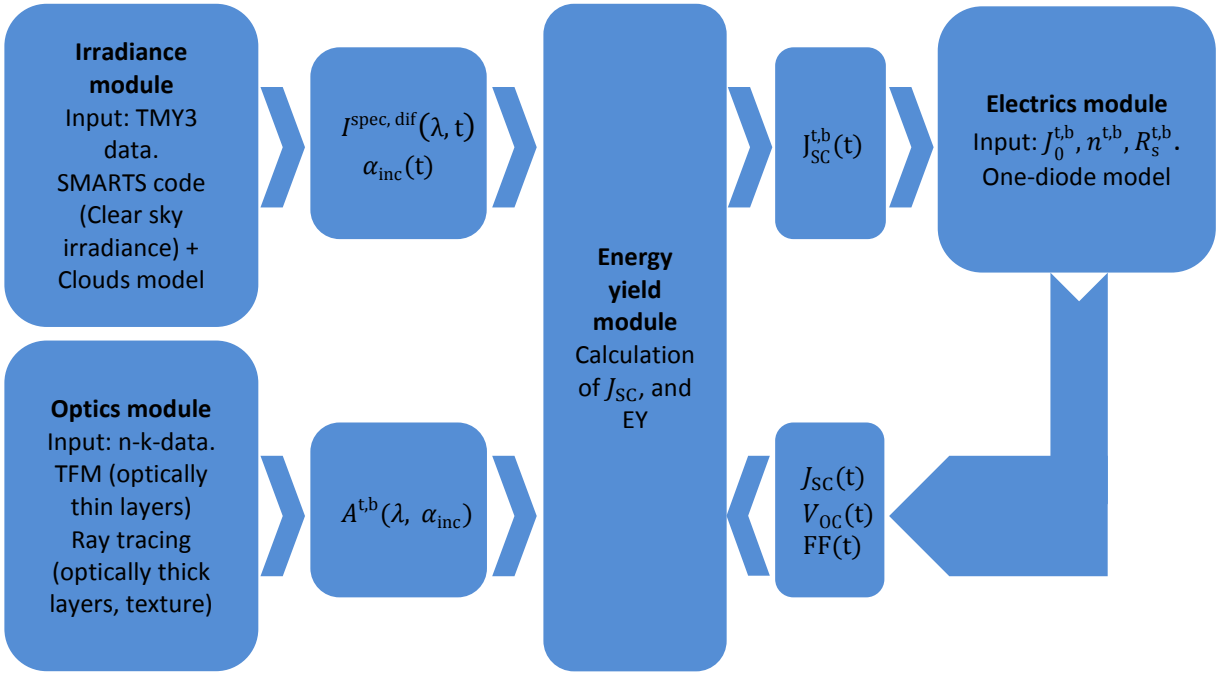


**Figure S1.** Schematic sketch of the software modules, showing handover of parameters and data for the calculation of energy yield (EY).

*Corresponding author *E-mail addresses*: jonathan.lehr@kit.edu (Jonathan Lehr), ulrich.paetzold@kit.edu (Ulrich W. Paetzold)
[†]These authors contributed equally to this work.

**Optics software module:** The perovskite/Si 2T tandem PV module layer stack consists of thin-film layer stacks (anti-reflection coating (ARC) and perovskite solar cell), which require rigorous coherent optical simulations, as well as "optically thick" layers (encapsulant, front glass, crystalline silicon (Si)) which can be treated by incoherent optics. The optics software module combines transfer-matrix method (TMM) for the coherent layer stacks and ray optics for those layers which are orders of magnitude thicker than the considered wavelength range (300 – 1200 nm). In the optically-thick layers, the absorption is calculated by applying a series expansion onto Lambert-Beer's law to account for multiple reflections. The calculated energy dissipation in the different absorber layers is subsequently used for determining the short-circuit current density ($J_{SC}$), assuming perfect charge carrier extraction efficiency. The textured surfaces are treated in the optical software module by statistical ray-tracing as described in literature for textured Si solar cells.[1,2] Our model determines rigorously the fraction of light transmitted into the Si absorber layer and further calculates the absorption in Si, assuming an effective light path enhancement as introduced by Yablonovitch *et al.* .[3] For perovskite/Si 2T tandem PV module architecture with double-side texture (case II), a light path enhancement factor Z = 25 was assumed, which is oriented at the lower limit of values from literature[4] to avoid over-estimations. For an architecture with texture at the rear side only (case III), we assume accordingly Z = 18.[5] For the architecture with both planar front and rear surfaces (case I), we assume Z = 2. It shall be noted, that the details about the layer stack at the rear electrode of the Si bottom solar cell are neglected, but indirectly considered via the light path enhancement factor.

**Irradiance software module:** The irradiance software module models the diffuse and specular irradiance spectra as well as the sun position for a given time and location. As a starting point, we use the typical meteorological year data sets (TMY3) available from the National Renewable Energy Laboratory (NREL).[6] This contains hourly resolved meteorological data and irradiance data as statistically representative over the time span of a year for many locations in the USA. Based on this data set, the direct and diffuse clear sky irradiance is determined using the "simple model of the atmospheric radiative transfer of sunshine" (SMARTS).[7] Subsequently, a simple fractional model of cloud coverage (data from TMY3) is applied, which assumes light transmitted through clouds to be equal in spectral distribution to direct clear sky irradiance. For specular irradiance, the incident angle is calculated using the sun's coordinates. Diffuse irradiance is assumed to be distributed as given by a Lambertian scatterer. The output of the irradiance software module provides the hourly resolved position of the sun as well as the specular and diffuse irradiance spectra for various locations in the USA.

**Electrics software module:** The electrics software module determines the *J-V* characteristics of the perovskite/Si 2T tandem PV modules for given $J_{SC}$ and temperature of the top and bottom solar cell. We use a common one-diode model based on the Shockley diode equation calculating the *J-V* characteristics of the subcells with the following equation

$$J(V) = J_{SC} - J_0 e^{\frac{V+JR_S}{nkT}}$$

with the input parameters $J_0$ dark saturation current density, n ideality factor, and $R_S$ series resistance for each subcell. The parametrization of these inputs is discussed later. Since the subcells of a 2T tandem solar cell are connected in series, the $J_{SC}$ of the limiting subcell is used as input $J_{SC}$ for the calculation of tandem solar cell. The output parameters FF, $V_{OC}$, and PCE of the tandem solar cell are calculated by determining the maximum power point of device.

**Energy yield software module:** This software module calculates finally the EY of perovskite/Si 2T tandem PV modules using inputs from all other software modules. First, for a given time and location, the $J_{SC}$ of the top and bottom solar cell are calculated based on the angular dependent external quantum efficiency (*EQE*), which is determined by the optics software module, and the diffuse and specular irradiance spectra, provided by the irradiance software module. For these calculations, the orientation of the perovskite/Si 2T tandem PV device with respect to the incident sun is explicitly considered. Having determined the $J_{SC}$, the MPP and the corresponding generated power of the perovskite/Si 2T tandem PV device is determined via the electrics software module. Our EY software module allows the comparison of the EY over arbitrary time spans and various locations in different climate zones. One-axis and two-axis tracking is also possible, though not explored in this study. The code can also be used to calculate the power conversion efficiency (PCE) under standard test conditions (STC), by assuming the irradiance spectrum to be the normalized air-mass 1.5 global (AM1.5g) reference spectrum.

**Device architecture, electrical parametrization and complex refractive indices:** The device architecture, the electrical parameters and the optical data of the investigated textured perovskite/Si 2T tandem PV modules were adapted from state-of-the-art reference devices. The selected device architecture of the textured perovskite/Si 2T tandem PV module uses exclusively materials that are also used in published perovskite/Si tandem solar cells.[8,9] However, alternative stacks might be equally representative, e.g. those using NiOx as hole transport material. The layer stack of the perovskite top solar cell mimics a widely used planar semi-transparent device architecture based on an indium tin oxide (ITO) front electrode, a titanium dioxide ($TiO_2$) electron transport layer, a perovskite absorber layer, a 2,2′,7,7′-tetrakis (N, N-di-p-methoxyphenylamino)-9,9′-spirobifluorene (Spiro-OMeTAD) hole transport layer and an ITO back electrode.[10] The opaque reference perovskite single-junction (SJ) solar cell, using the same architecture but with a gold (Au) back electrode and the same electrical parameters, exhibits a PCE of around 17.9% (refer Figure S2), which is close to the record PCE for perovskite solar cells of bandgap around 1.72 eV.[11] The electrical parameters of the Si bottom solar cell are adapted from the current world record crystalline Si SJ solar cell.[12] We use $J_0$ of $1x10^{-14}$ mA/cm$^2$, $n$ of 0.82 and $R_S$ of 0.1 Ω as electrical input parameters in the one-diode model of the Si bottom solar cell, in order to quantitatively reproduce the open-circuit voltage ($V_{OC}$) and fill factor (FF) from experiment (see Figure S5). Although the architecture of this interdigitated back contact (IBC) record device is not directly compatible with the 2T tandem architecture, we select the forward-looking electrical parameters. The applied layer sequence of the crystalline Si bottom solar cell mimics the front side of a conventional crystalline Si SHJ solar cell based on a Si wafer absorber, a hydrogenated amorphous Si passivation layer, an ITO front electrode and a magnesium fluoride ($MgF_2$) ARC. As described above, the absorption in the Si absorber is treated by an effective light path enhancement factor, which also indirectly includes the effect of parasitic absorption at the rear side electrode and rear side passivation layer. For the opaque reference Si SJ solar cell employing these electrical parameters and the above described layer sequence, a PCE of 24.3% was calculated (as shown in Figure S5). The apparent discrepancy in PCE between the IBC record device[12] and our PCE is simply founded in the modified layer stack and more moderate assumptions about the light path enhancement in this work. For all architectures, an encapsulant (EVA) and module cover glass (low iron starphire) as well as an $MgF_2$ ARC for reduction of front side reflection was applied at the top of, both, perovskite/Si 2T tandem solar cell and Si SJ reference.

The complex refractive indices of each material are taken from established references ($MgF_2$,[13] glass,[14] encapsulant,[15] front ITO,[16] $TiO_2$,[16] Spiro-OMeTAD,[16] rear ITO,[16] hydrogenated amorphous Si,[17] crystalline Si[18]), as well as in-house values for other layers (multicrystalline metal-halide perovskite layer with various compositions and bandgaps of 1.55 eV,[16] 1.66 eV (in-house), 1.72 eV (in-house), 1.80 eV,[19] and 1.88 eV[19]). All used complex refractive indices are also shown in the Figures S6 – S12.

The one-diode model used in the electrics software module relies on the input of $J_0$, $n$, and $R_S$. As described above, for the crystalline Si bottom solar cell, these inputs are adapted from the current world record crystalline Si SJ solar cell (see Figure S5).[12] For the perovskite top solar cell, the following set of electrical parameters is used reproducing $V_{OC}$, FF, and PCE of experimental *J-V* characteristics of state-of-the-art perovskite solar cells (see also Figures S2 and S3). Depending on the bandgap of the perovskite absorber layer the $J_0$, and the $R_S$ are expected to vary due to changing free charge carrier density and recombination.[20] In accordance with previous studies by Hörantner *et al.*,[20] for the bandgaps introduced above (1.55 eV, 1.66 eV, 1.72 eV, 1.8 eV, 1.88 eV), we use $J_0$ values of $3x10^{-11}$ mA/cm$^2$, $1x10^{-13}$ mA/cm$^2$, $8x10^{-15}$ mA/cm$^2$, $2x10^{-16}$ mA/cm$^2$ and $2x10^{-18}$ mA/cm$^2$, respectively. We use corresponding $R_S$ values of 4.1 Ω, 7.4 Ω, 8.9 Ω, 12.4 Ω, and 16.9 Ω, as well as a constant $n$ value of 1.43 in order to ensure that the $V_{OC}$ of perovskite top solar cell varies linearly with bandgap. For the simulated perovskite/Si 2T tandem PV module the resulting $V_{OC}$ varies also almost linearly with bandgap, since the subcells are connected in series. The predicted $V_{OC}$ values for the double-side textured perovskite/Si 2T tandem PV module are 1.69 V, 1.89 V, 1.98 V, 2.11 V, 2.24 V, respectively.

Figures and Tables

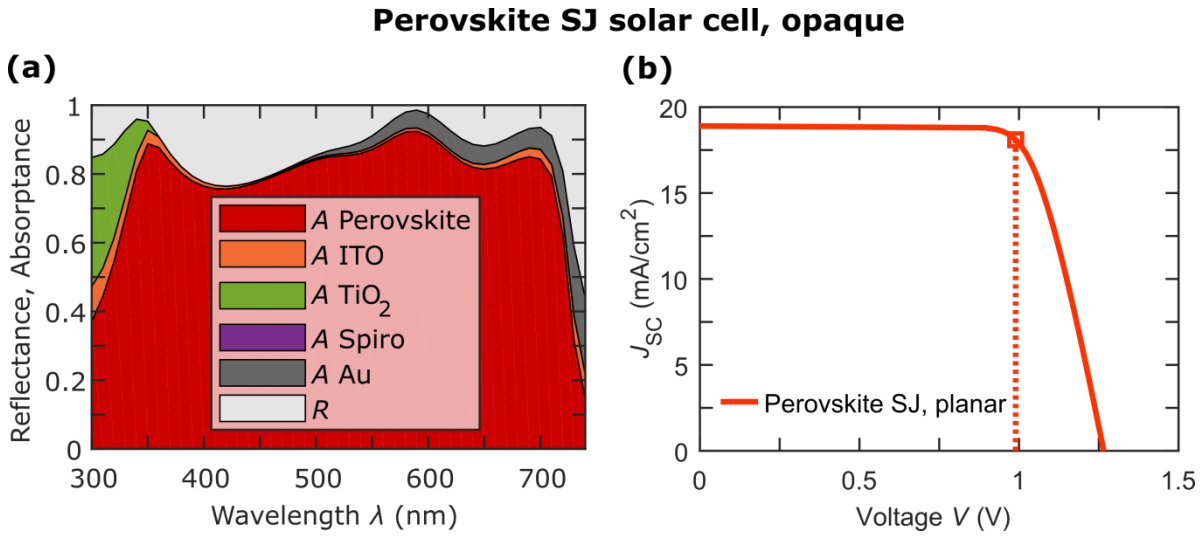


| Layer | Thickness $d$ (nm) |
|---|---|
| ITO | 75 |
| $TiO_2$ | 20 |
| Perovskite 1.72 eV | 390 |
| Spiro-OMeTAD | 20 |
| Au | 100 |

| $V_{OC}$ (V) | FF | $J_{SC}$ (mA/cm$^2$) | PCE |
|---|---|---|---|
| 1.27 | 0.75 | 18.9 | 17.9% |

**Figure S2.** (a) Optical and (b) electrical properties of opaque perovskite SJ solar cell with Au back electrode, used as starting point for the simulation of perovskite/Si 2T tandem PV modules. The presented values of PCE, $V_{OC}$, FF, and $J_{SC}$ are rounded for reasons of clarity.

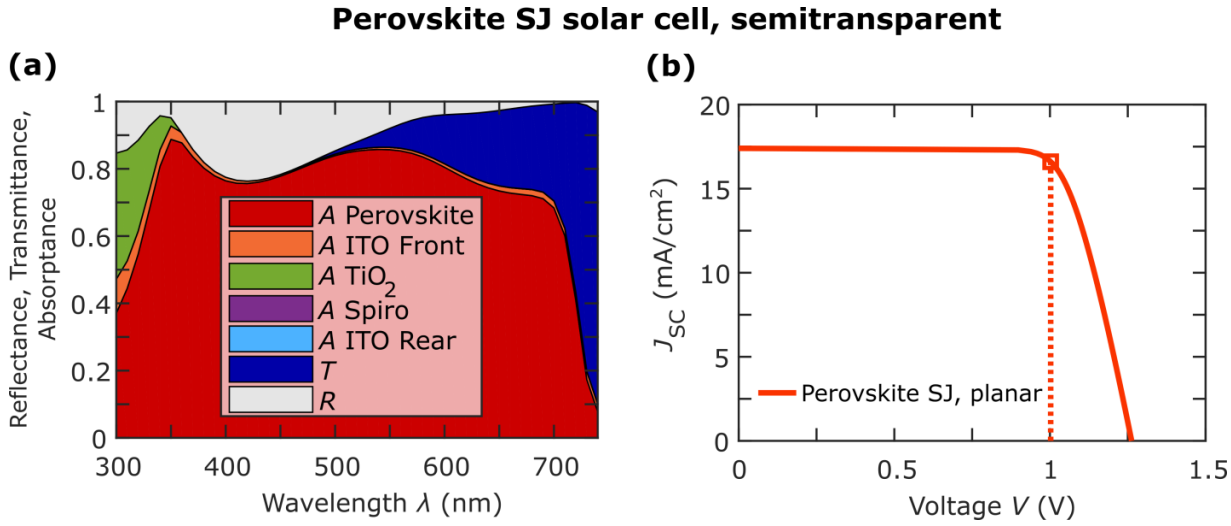


| Layer | Thickness $d$ (nm) |
|---|---|
| ITO | 75 |
| $TiO_2$ | 20 |
| Perovskite 1.72 eV | 390 |
| Spiro-OMeTAD | 20 |
| ITO | 10 |

| $V_{OC}$ (V) | FF | $J_{SC}$ (mA/cm$^2$) | PCE |
|---|---|---|---|
| 1.26 | 0.76 | 17.3 | 16.6% |

**Figure S3.** (a) Optical and (b) electrical properties of perovskite SJ solar cell with transparent ITO back electrode, used for the simulation of perovskite/Si 2T tandem solar cells and PV modules. The presented values of PCE, $V_{OC}$, FF, and $J_{SC}$ are rounded for reasons of clarity.

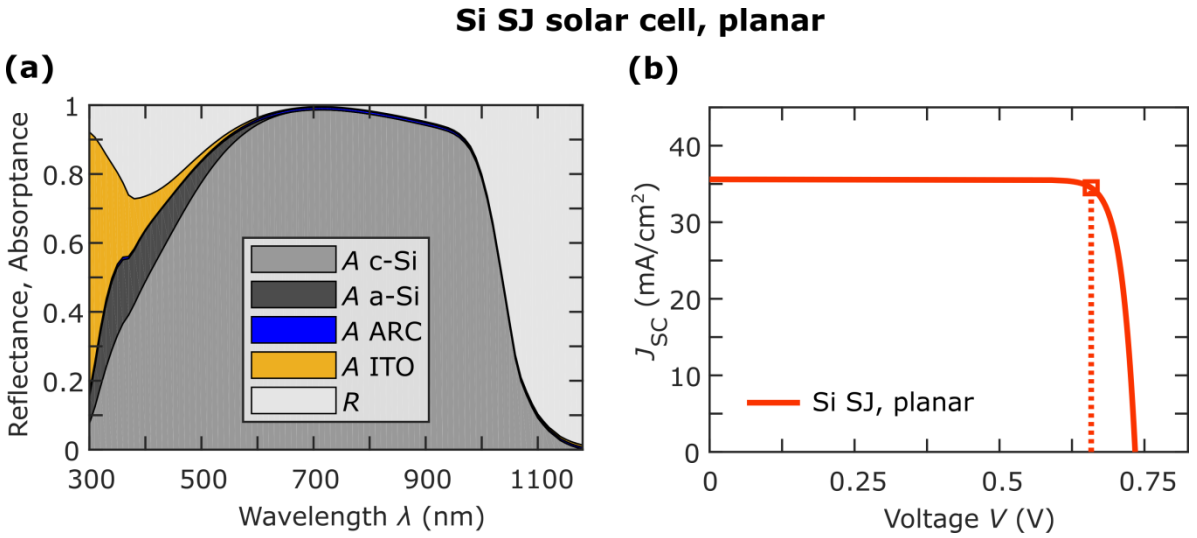


| Layer | Thickness $d$ (nm) |
|---|---|
| MgF2 | 60 |
| ITO | 70 |
| a-Si | 10 |
| c-Si | 160000 |

| $V_{OC}$ (V) | FF | $J_{SC}$ (mA/cm$^2$) | PCE |
|---|---|---|---|
| 0.73 | 0.87 | 35.5 | 22.7% |

**Figure S4.** (a) Optical and (b) electrical properties of Si SJ solar cell with planar architecture, used for the simulation of perovskite/Si 2T tandem solar cells and PV modules. The presented values of PCE, $V_{OC}$, FF, and $J_{SC}$ are rounded for reasons of clarity.

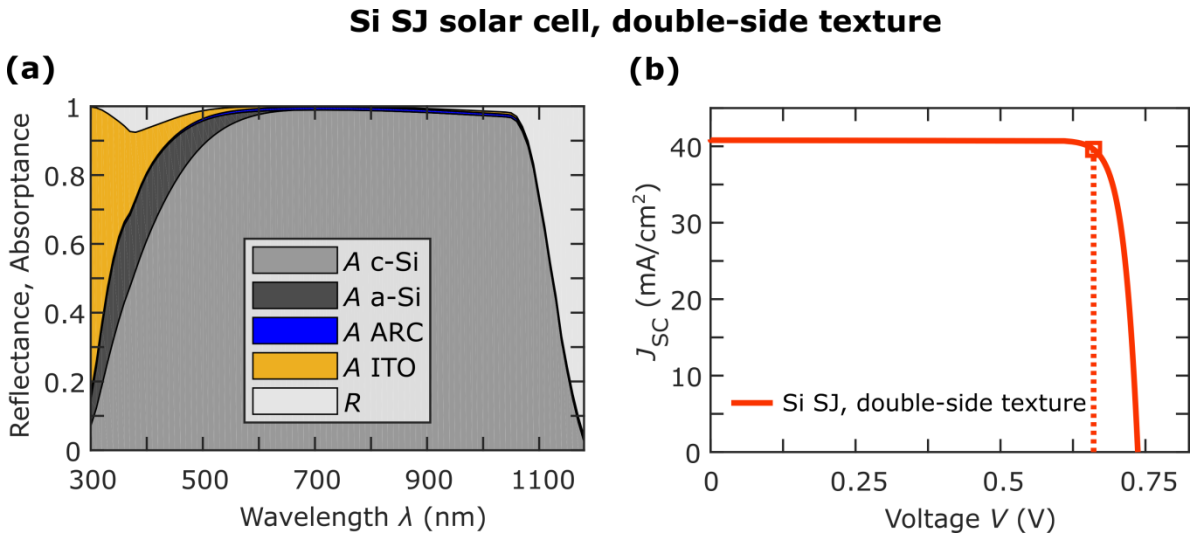


| Layer | Thickness $d$ (nm) |
|---|---|
| $MgF_2$ | 60 |
| ITO | 70 |
| a-Si | 10 |
| c-Si | 160000 |

| $V_{OC}$ (V) | FF | $J_{SC}$ (mA/cm$^2$) | PCE |
|---|---|---|---|
| 0.74 | 0.81 | 40.8 | 24.3% |

**Figure S5.** (a) Optical and (b) electrical properties of Si SJ solar cell with double-side texture, used for the simulation of perovskite/Si 2T tandem solar cells and PV modules. The presented values of PCE, $V_{OC}$, FF, and $J_{SC}$ are rounded for reasons of clarity.

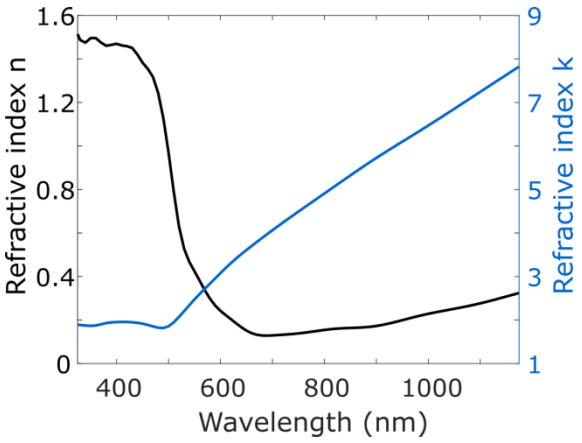


**Figure S6.** Optical constants of Au, used as input for the optical analysis as well as the full simulation of solar cells and PV modules.

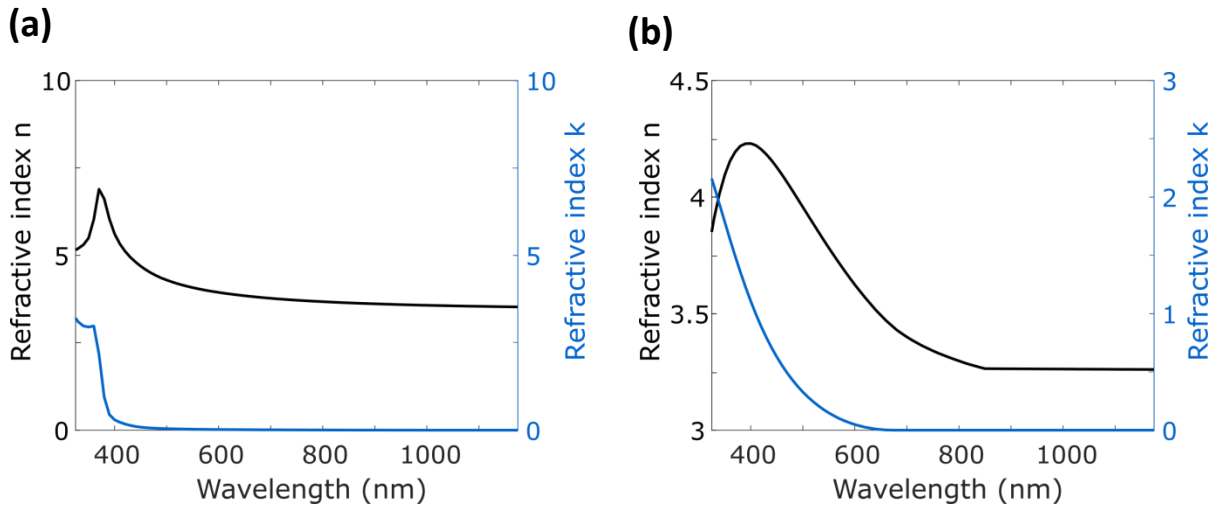


**Figure S7.** Optical constants of (a) crystalline Si, and (b) amorphous Si, used as input for the optical analysis as well as the full simulation of solar cells and PV modules.

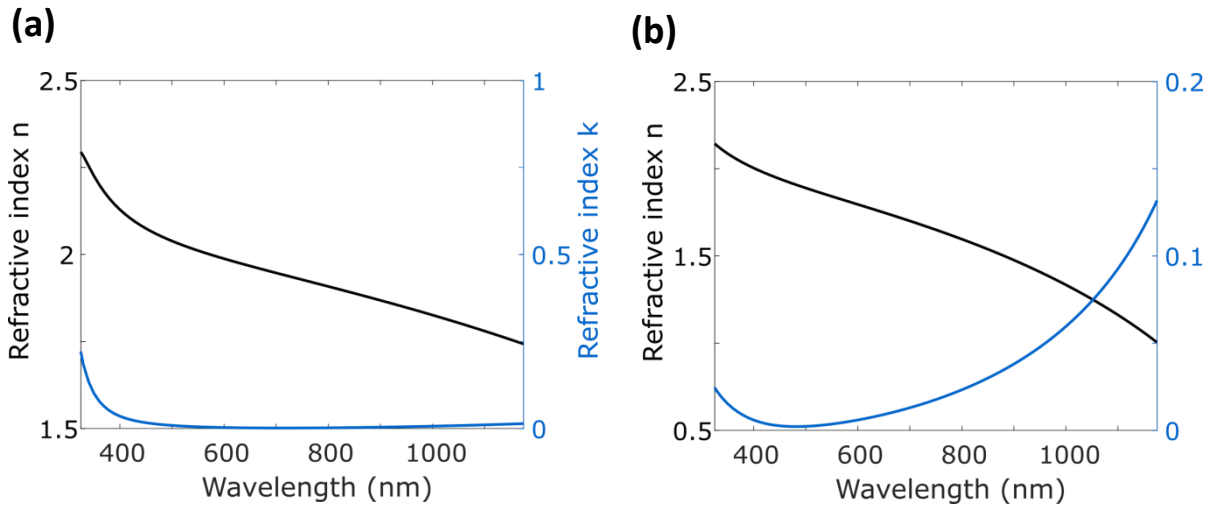


**Figure S8.** Optical constants of (a) ITO for recombination layer, and (b) ITO for transparent front electrode, used as input for the optical analysis as well as the full simulation of solar cells and PV modules.

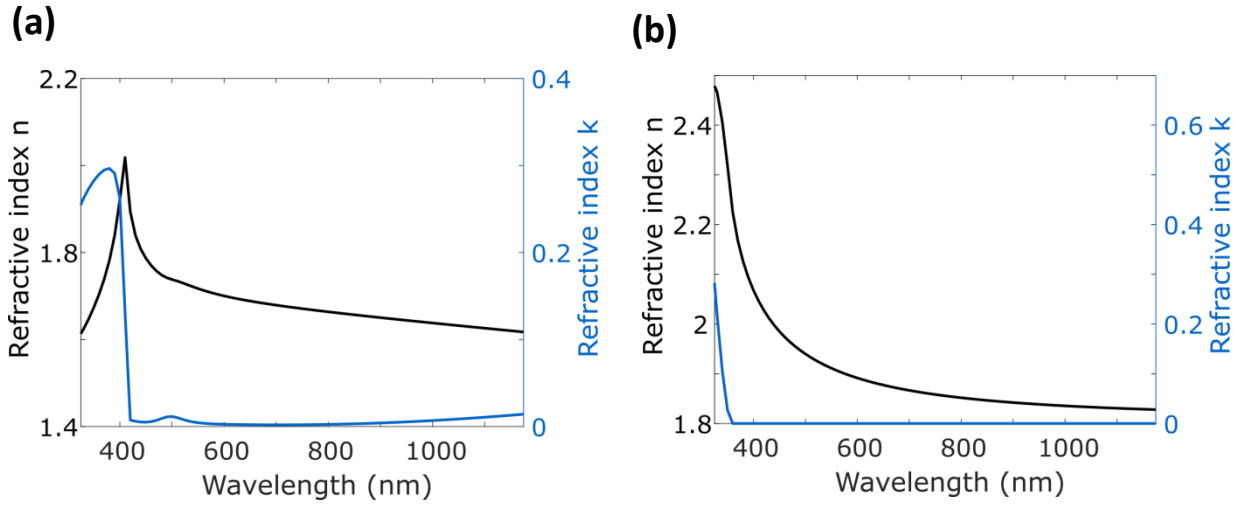


**Figure S9.** Optical constants of (a) Spiro-OMeTAD, and (b) $TiO_2$, used as input for the optical analysis as well as the full simulation of solar cells and PV modules.

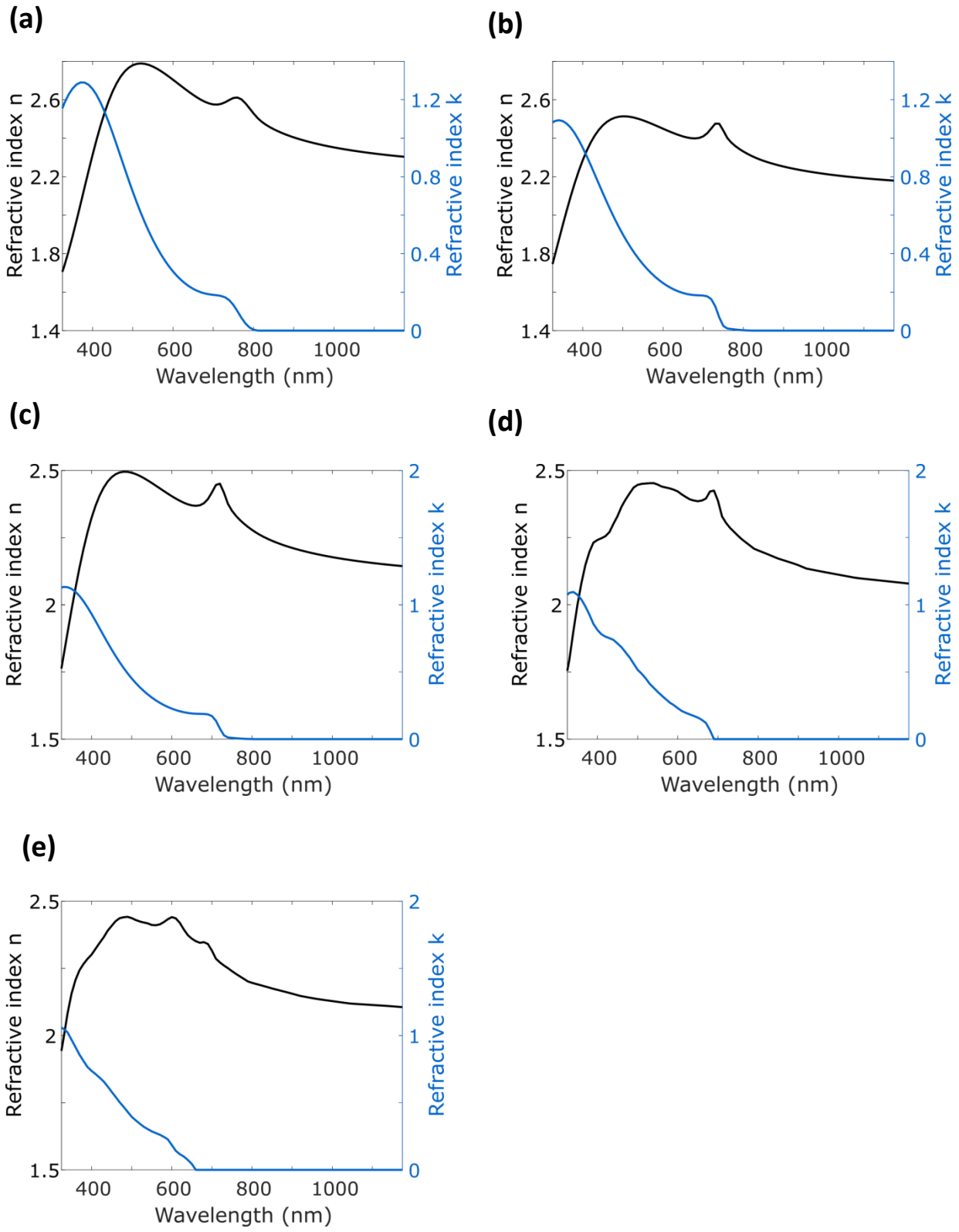


**Figure S10.** Optical constants of Perovskite with bandgap of (a) 1.55 eV, (b) 1.66 eV, (c) 1.72 eV, (d) 1.80 eV, and (e) 1.88 eV, used as input for the optical analysis as well as the full simulation of solar cells and PV modules.

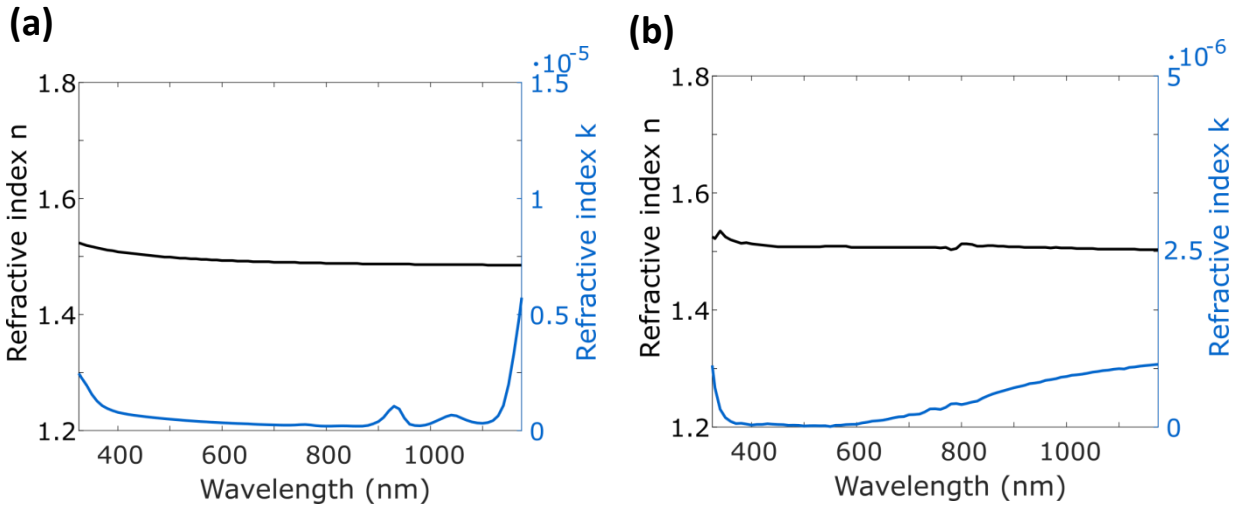


**Figure S11.** Optical constants of (a) encapsulation, and (b) glass, used as input for the optical analysis as well as the full simulation of solar cells and PV modules.

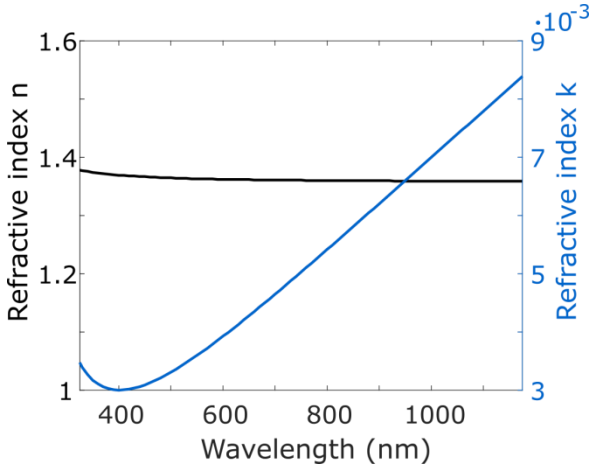


**Figure S12.** Optical constants of $MgF_2$, used as input for the optical analysis as well as the full simulation of solar cells and PV modules.

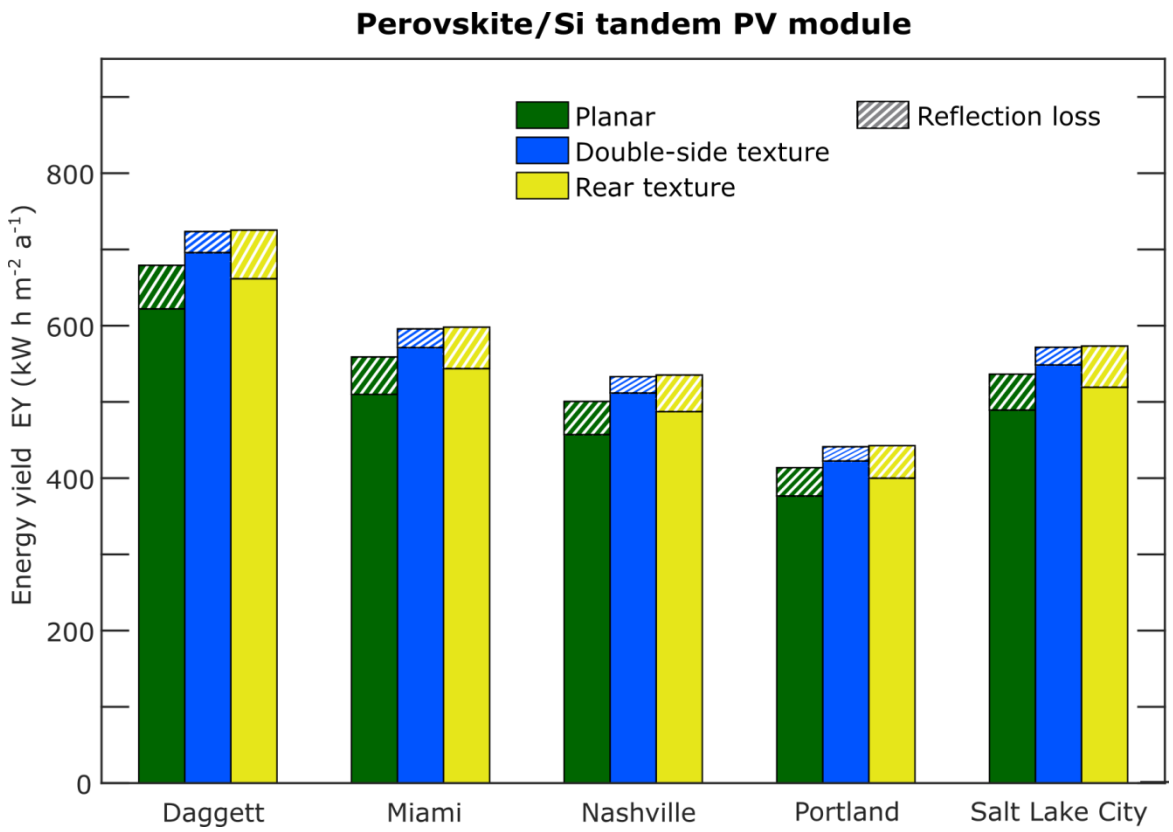


**Figure S13.** Reflection loss in EY for the investigated perovskite/Si 2T tandem PV module architectures namely planar, double-side texture, and rear texture. The losses are calculated by recalculating the EY under the assumption of negligible reflectance, i.e. $A_{per,R=0} = A_{per} / (1-R_{front})$, $A_{Si,R=0} = A_{Si} / (1-R_{front})$. The reflectance at the front $R_{front}$ is used rather than the total reflectance, as Si absorbs light imperfectly for wavelengths > 950nm and the amount of light reflected back from the Si back contact shall not be considered for the investigation of the impact of front side reflection on the EY. Since the absorption in the Si absorber layer is calculated with an effective light path enhancement (see section Methods of supplementary), we assume complete absorption of all light transmitted into Si. As a result the calculated loss is underestimated for the planar architecture with its distinct low light path enhancement factor. The reflection loss is provided for five locations Daggett (California), Miami (Florida), Nashville (Tennessee), Portland (Oregon), and Salt Lake City (Utah), with optimized PV module tilt angle and optimized perovskite absorber layer thickness for each location.

| Architecture | Location | Efficiency de-rating factor |
|---|---|---|
| Planar | Daggett | 1.02 |
| | Miami | 1.04 |
| | Nashville | 1.03 |
| | Portland | 1.03 |
| | Salt Lake City | 1.03 |
| Double-side texture | Daggett | 0.96 |
| | Miami | 0.98 |
| | Nashville | 0.96 |
| | Portland | 0.96 |
| | Salt Lake City | 0.97 |
| Rear side texture | Daggett | 1.00 |
| | Miami | 1.03 |
| | Nashville | 1.01 |
| | Portland | 1.00 |
| | Salt Lake City | 1.00 |

**Table S1.** Efficiency de-rating factors of perovskite/Si 2T tandem PV modules with metal-halide perovskite of bandgap 1.72 eV at optimal perovskite absorber layer thickness and optimal tilt angle. The efficiency de-rating factors are calculated for perovskite/Si 2T tandem PV modules with planar architecture, double-side texture, and rear side texture, as well as for the locations Daggett, Miami, Nashville, Portland and Salt Lake City.

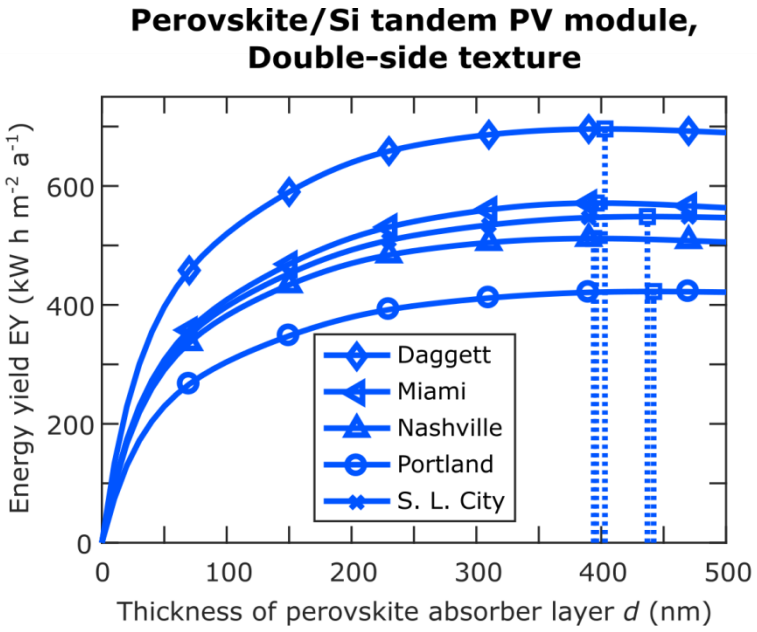


**Figure S14.** EY of perovskite/Si 2T tandem PV module with metal-halide perovskite of bandgap 1.72 eV, as a function of perovskite absorber layer thickness. The EY is provided for five locations Daggett, Miami, Nashville, Portland, and Salt Lake City, at optimized tilt angle of PV module for each location.

## References


1 S. C. Baker-Finch and K. R. McIntosh, *Prog. Photovoltaics Res. Appl.*, 2011, **19**, 406–416.

2 K. R. McIntosh and S. C. Baker-Finch, in *38th IEEE Photovoltaic Specialists Conference*, 2012, 265–271.

3 E. Yablonovitch and G. D. Cody, *IEEE Trans. Electron Devices*, 1982, **29**, 300–305.

4 P. Campbell and M. A. Green, *J. Appl. Phys.*, 1987, **62**, 243–249.

5 J. A. Rand and P. A. Basore, in *The Conference Record of the Twenty-Second IEEE Photovoltaic Specialists Conference*, 1991, 192–197.

6 S. Wilcox and W. Marion, *Renew. Energy*, 2008, 51.

7 C. A. Gueymard, *Sol. Energy*, 2001, **71**, 325–346.

8 F. Sahli, J. Werner, B. A. Kamino, M. Bräuninger, R. Monnard, B. Paviet-Salomon, L. Barraud, L. Ding, J. J. D. Leon, D. Sacchetto, G. Cattaneo, M. Boccard, M. Despeisse, S. Nicolay, Q. Jeangros, B. Niesen and C. Ballif, *Nat. Mater.*, 2018, **17**, 820-826.

9 Y. Wu, D. Yan, J. Peng, T. Duong, Y. Wan, S. P. Phang, H. Shen, N. Wu, C. Barugkin, X. Fu, S. Surve, D. Grant, D. Walter, T. P. White, K. R. Catchpole and K. J. Weber, *Energy Environ. Sci.*, 2017, **10**, 2472–2479.

10 M. Jaysankar, M. Filipic, B. Zielinski, R. Schmager, W. Song, W. Qiu, U. W. Paetzold, T. Aernouts, M. Debucquoy, R. Gehlhaar and J. Poortmans, *Energy Environ. Sci.*, 2018, **11**, 1489-1498.

11 X. Li, D. Bi, C. Yi, J.-D. Décoppet, J. Luo, S. M. Zakeeruddin, A. Hagfeldt and M. Grätzel, *Science*, 2016, **353**, 58-62.

12 K. Yoshikawa, H. Kawasaki, W. Yoshida, T. Irie, K. Konishi, K. Nakano, T. Uto, D. Adachi, M. Kanematsu, H. Uzu and K. Yamamoto, *Nat. Energy*, 2017, **2**, 17032.

13 J. M. Siqueiros, R. Machorro and L. E. Regalado, *Appl. Opt.*, 1988, **27**, 2549.

14 K. R. McIntosh, L. Gay, J. N. Cotsell, K. Hanton, D. L. Bätzner, F. Bettiol and B. S. Richards, *Prog. Photovoltaics Res. Appl.*, 2009, **17**, 191–197.

15 M. R. Vogt, H. Holst, H. Schulte-Huxel, S. Blankemeyer, R. Witteck, D. Hinken, M. Winter, B. Min, C. Schinke, I. Ahrens, M. Köntges, K. Bothe and R. Brendel, *Energy Procedia*, 2016, **92**, 523–530.

16 M. van Eerden, M. Jaysankar, A. Hadipour, T. Merckx, J. J. Schermer, T. Aernouts, J. Poortmans and U. W. Paetzold, *Adv. Opt. Mater.*, 2017, **5**, 1–10.

17 Z. C. Holman, a. Descoeudres, L. Barraud, F. Z. Fernandez, J. P. Seif, S. De Wolf and C. Ballif, *IEEE J. Photovoltaics*, 2012, **2**, 7–15.

18 M. a. Green, *Sol. Energy Mater. Sol. Cells*, 2008, **92**, 1305–1310.

19 P. F. Ndione, Z. Li and K. Zhu, *J. Mater. Chem. C*, 2016, **4**, 7775–7782.

20 M. T. Hörantner and H. Snaith, *Energy Environ. Sci.*, 2017, **10**, 1983–1993.